Published in final edited form as:
J Bone Miner Res. 2013 September ; 28(9): 1885–1897. doi:10.1002/jbmr.1943.

Altered thermogenesis and impaired bone remodeling in *Misty* mice

Katherine J Motyl[1], **Kathleen A Bishop**[1], **Victoria E DeMambro**[1], **Sheila A Bornstein**[1], **Phuong Le**[1], **Masanobu Kawai**[1,2], **Sutada Lotinun**[3], **Mark C Horowitz**[4], **Roland Baron**[3], **Mary L Bouxsein**[5], and **Clifford J Rosen**[1]

[1]Center for Clinical and Translational Research, Maine Medical Center Research Institute, Scarborough, ME, USA

[2]Department of Bone and Mineral Research, Osaka Medical Center and Research Institute for Maternal and Child Health, Izumi, Osaka, Japan

[3]Department of Medicine, Harvard Medical School, Harvard School of Dental Medicine, Harvard University, Boston, MA, USA

[4]Department of Orthopaedics and Rehabilitation, Yale University School of Medicine, New Haven, CT, USA

[5]Department of Orthopedic Surgery, Beth Israel Deaconess Medical Center and Harvard Medical School, Boston, MA, USA

Abstract

Fat mass may be modulated by the number of brown-like adipocytes in white adipose tissue (WAT) in humans and rodents. Bone remodeling is dependent on systemic energy metabolism and, with age, bone remodeling becomes uncoupled and brown adipose tissue (BAT) function declines. To test the interaction between BAT and bone, we employed *Misty (m/m)* mice, which were reported be deficient in BAT. We found that *Misty* mice have accelerated age-related trabecular bone loss and impaired brown fat function (including reduced temperature, lower expression of *Pgc1a* and less sympathetic innervation compared to wildtype (*+/+*)). Despite reduced BAT function, *Misty* mice had normal core body temperature, suggesting heat is produced from other sources. Indeed, upon acute cold exposure (4°C for 6 hr), inguinal WAT from *Misty* mice compensated for BAT dysfunction by increasing expression of *Acadl*, *Pgc1a*, *Dio2* and other thermogenic genes. Interestingly, acute cold exposure also decreased *Runx2* and increased *Rankl* expression in *Misty* bone, but only *Runx2* was decreased in wildtype. Browning of WAT is under the control of the sympathetic nervous system (SNS) and, if present at room temperature, could impact bone metabolism. To test whether SNS activity could be responsible for accelerated trabecular bone loss, we treated wildtype and *Misty* mice with the β-blocker, propranolol. As predicted, propranolol slowed trabecular BV/TV loss in the distal femur of *Misty* mice without affecting wildtype. Finally, the *Misty* mutation (a truncation of DOCK7) also has a significant cell-autonomous role. We found DOCK7 expression in whole bone and osteoblasts. Primary osteoblast differentiation from *Misty* calvaria was impaired, demonstrating a novel role for DOCK7 in bone remodeling. Despite the multifaceted effects of the *Misty* mutation, we have

Address correspondence and requests for reprints to: Dr. Katherine J Motyl, Maine Medical Center Research Institute, 81 Research Drive, Scarborough, ME, 04074-7205, USA, TEL: +1-207-396-8004, FAX: +1-207-396-8110, motylk@mmc.org.

Disclosures: All authors state that they have no conflicts of interest.

KJM, KAB, VED, MK, and MLB contributed to design, data acquisition, analysis and interpretation. SAB, PL, SL contributed to data acquisition, analysis and interpretation. MCH, RB and CJR contributed to design and interpretation. KJM and MK drafted the initial manuscript and the remaining authors critically revised the manuscript. All authors approved the final version of the manuscript.

shown that impaired brown fat function leads to altered SNS activity and bone loss, and for the first time that cold exposure negatively affects bone remodeling.

Keywords

bone; brown adipose tissue; DOCK7; *Misty*; thermogenesis

Introduction

Control of energy balance is a highly integrated part of metabolism and involves a number of tissues including the hypothalamus, white adipose tissue (WAT) and brown adipose tissue (BAT). In addition, emerging evidence indicates that skeletal metabolism is regulated by systemic energy balance (1–3). For example, leptin is released from WAT when there is excess energy and signals to the hypothalamus to increase energy expenditure and reduce appetite (4, 5). Evidence suggests that leptin also decreases skeletal mass through a hypothalamic-sympathetic relay by uncoupling bone remodeling units leading to suppressed bone formation and enhanced bone resorption (6–8). Consistent with this, sympathetic signaling through the β2-adrenergic receptor (β2AR) results in bone loss (9). Interestingly, the skeleton in turn regulates the expression of insulin and adiponectin in pancreatic β-cells and adipocytes, respectively, by modulating the ratio of un- and under-carboxylated osteocalcin (OCN) relative to total osteocalcin (10). These lines of evidence suggest that energy and skeletal metabolism are mutually interactive and that the sympathetic nervous system (SNS) is critical in this network.

BAT is essential for energy homeostasis in rodents, hibernating animals and neonates. Accumulating evidence from clinical studies suggests the presence of functional BAT in adult humans, although its role in modulating energy metabolism is not clear (11–14). In neonates and small animals such as rodents, BAT contributes to the maintenance of core body temperature and adaptive thermogenesis in response to external stimuli such as food intake and cold exposure. In rodents, a defect in BAT function often results in low body temperature and intolerance to cold exposure due to impaired adaptive thermogenesis. However, the SNS compensates for the lack of BAT in an attempt to maintain body temperature. For example, in adult *Ucp1*$^{-/-}$ mice, there is no functional BAT, but SNS tone is enhanced, WAT appears ‘brown-like’, and body temperature is maintained at thermo-neutrality (15). Similarly, stimulation of the SNS by treatment with a β3-adrenergic receptor agonist increases metabolic rate in peripheral tissues including WAT (16, 17), and an elevated metabolic rate in WAT causes a morphological change of white adipocytes into brown-like adipocytes accompanied by an increase in mitochondrial content. Thus, elevated sympathetic tone induced by BAT dysfunction causes increased energy expenditure in the peripheral WAT leading to a lean phenotype and a greater metabolic rate. However, increased energy expenditure cannot fully compensate for low body temperature because the thermogenic capacity of peripheral tissues is not as efficient as that in BAT. Thus, BAT plays an important role in energy metabolism in collaboration with the hypothalamic-sympathetic network and affects the systemic alteration of body composition.

The relationship of BAT function to skeletal metabolism in rodents has not previously been studied. Interestingly, in a recent study of younger women, Bredella and colleagues demonstrated a strong positive correlation between BAT volume (by PET) and bone mineral density (18). Similar findings in adolescents were noted by Ponrartana et al, although the correlation became non-significant when muscle mass was included in a multiple regression analysis (19). Notwithstanding, because the sympathetic nervous system regulates skeletal metabolism in a negative manner, we hypothesized that BAT dysfunction drives the SNS

and leads to bone loss due to the disruption of the bone remodeling unit (20). To shed light on this issue, we took advantage of *Misty* mice, which have reduced BAT function, and analyzed their skeletal phenotype (21). The diluted coat color and white belly spot of *Misty* mice were originally used as a phenotypic marker for the prediction of the *Lepr* (*db*) genotype because *Lepr* (*db*) locus co-segregates with the locus affected by the *Misty* mutation. Recently, DOCK7, a Rho family guanine exchange factor (GEF) belonging to the DOCK180 protein family, which has been implicated in axon formation and Schwann cell migration (22, 23), was reported to be responsible for the phenotype of *Misty* mice (24). DOCK7 is a 2130 amino acid protein and is involved in the function of Rho family of small GTPase such as Rac1, cdc42 and RhoA (25). DOCK7 contains the evolutionarily conserved Dock homology region (DHR)-1 and DHR-2 domains (25–27). The DHR-2 domain has been shown to be necessary for the exchange of GDP to GTP on the GTPases, whereas the DHR-1 domain has been implicated in the interaction with phosphatidylinositol (3,5)-bisphosphate (25–27). *Misty* mice possess a 43-bp insertion in Exon18, which generates a premature stop codon (24). The truncation occurs in the middle of the DHR-1 domain and if translated, the truncated *Misty* protein would completely lack the DHR-2 domain (24). Therefore, the *Misty* mutation in DOCK7 is likely a loss of function mutation although this awaits confirmatory studies.

In this study we demonstrate that the *Misty* mice have accelerated age-dependent trabecular bone loss due to impaired bone formation and increased bone resorption in both a cell and non-cell autonomous manner. In respect to the latter, trabecular bone loss in *Misty* mice was slowed by treatment with a β-adrenergic receptor antagonist. These lines of evidence demonstrate that BAT function is involved in skeletal metabolism in part through modulating the SNS.

Materials and Methods

Mice

B6.D2(BKS)-*Dock7*$^{m/m}$ mice, which we refer to as *Misty* (*m/m*) mice, were purchased from Jackson Laboratory (Bar Harbor, Maine). *Misty* mice were backcrossed to C57BL/6J (Jackson Laboratory) and bred as heterozygous matings to produce *Misty* mice and wildtype littermate controls. All animal studies were reviewed and approved by the Institutional Animal Care and Use Committee of Maine Medical Center Research Institute.

Dual-energy X-ray absorptiometry (DXA)

Dual-energy X-ray absorptiometry (DXA) for whole body and femoral areal bone mineral density (aBMD, g/cm^2) and body composition exclusive of the head were performed using the PIXImus (GE-Lunar) as previously described (28). The PIXImus was calibrated daily with a phantom provided by the manufacturer.

MicroCT

Microarchitecture of distal trabecular bone and midshaft cortical bone were analyzed in femora and vertebrae (L5) by high resolution micro-computed tomography (resolution 10 μm, VivaCT-40, Scanco Medical AG, Bassersdorf, Switzerland). Bones were scanned at energy level of 55 kVp, and intensity of 145 μA. The VivaCT-40 is calibrated weekly using a phantom provided by Scanco. Trabecular bone volume fraction and micro-architecture were evaluated in the secondary spongiosa, starting proximately at 0.6 mm proximal to the distal femoral growth plate, and extending proximally 1.5 mm. Approximately 230 consecutive slices were made at 10.5 μm interval at the distal end of the growth plate and extending in a proximal direction, and 180 contiguous slices were selected for analysis. A fixed threshold of 220 was used to separate bone from soft tissue in all samples.

Measurements included trabecular bone volume/total volume (Tb.BV/TV), trabecular number (Tb.N), trabecular thickness (Tb.Th), trabecular separation (Tb.Sp.) and connectivity density. Scans for the cortical region were measured at the mid-point of each femur, with an isotropic pixel size of 21 μm and slice thickness of 21 μm, and used to calculate the average bone area (BA), total cross-sectional area (TA), bone area/total area (BA/TA), and cortical thickness (Ct.Th.). For mid-shaft analysis, the cortical shell was contoured by user-defined threshold of 260 and iterated through all 50 slices. All scans were analyzed using manufacturer software (Scanco, version 4.05). Acquisition and analysis of microCT data were performed in accordance with recently published guidelines (29).

Bone Histomorphometry

Static and dynamic histomorphometry measures were analyzed between *Misty* and control mice at 16 weeks of age. Mice were injected with 20 mg/kg calcein and demeclocycline intraperitoneally 7 days and 2 days, respectively, before sample collection. Femurs were analyzed as described previously (28) and standard nomenclature was used (30).

Adipose Tissue Histology and Immunohistochemistry

Brown adipose tissue was fixed in 10% neutral buffered formalin and then transferred to 70% ethanol after 24 hours. Samples were paraffin embedded, sectioned and stained with hematoxylin and eosin. Anti-UCP1 (ab23841) and anti-tyrosine hydroxylase (TH, ab112) antibodies were purchased from Abcam (Cambridge, MA). TH stain: unstained paraffin embedded sections were incubated for 1 hr at room temperature with a 1:700 dilution of anti-TH primary antibody or overnight at 4°C with a 1:250 dilution of anti-UCP-1 primary antibody and developed using the Vectastain ABC kit (Vector Laboratories, Burlingame, CA).

Analysis of Body Temperature

Thermal Signature Analysis ImagIR (Seahorse Bioscience, North Billerica, MA, performed by JAX Phenotyping Services, The Jackson Laboratory, Bar Harbor, ME) was used for the analysis of interscapular thermal change in response to intraperitoneal administration of β3 adrenergic receptor agonist (1.0 mg/kg BW, BRL 37344) according to the manufacturer's protocol. Body temperature was monitored for 90 minutes after the injection of BRL 37344. Core (rectal) temperature was measured with a ThermoWorks Microtherma 2 (Alpine, UT).

Cold Exposure

Wildtype and *Misty* mice were subjected to 4°C temperatures (in previously cooled cages containing standard bedding, food and water) for six hours. Mice were observed every 15 minutes for signs of distress. Rectal temperature was monitored every hour.

Brown Adipocyte Culture

Primary brown adipocytes from wildtype and *Misty* mice were isolated from the interscapular preformed brown adipose tissue (BAT) of neonates (P3) and cultured with modifications according to previously published protocols (31–33). Briefly, BAT was excised and minced under sterile conditions and incubated with isolation buffer (0.123 M NaCl, 1.3 mm $CaCl_2$, 5 mM glucose, 100 mM Hepes, 4% BSA and 0.1% collagenase P) for 40 min at 37°C. Cells were washed and resuspended in primary culture medium (high glucose DMEM, 20% FBS and 1% Penn Strep) and plated at 20,000 cells/cm^2. Cells were maintained in primary culture medium (with daily media changes) until confluence, at which time they were trypsinized and plated at 4,000 cells/cm^2 in differentiation media (high glucose DMEM, 10% FBS, 20 nM insulin and 1 nM triiodo-L-thyronine (T3)), changed every other day. At confluence, media was changed to induction media (differentiation

media, 0.125 mM indomethacin, 0.5 mM IBMX and 5 μM dexamethasone) for two days. Cells were then changed back to differentiation media and maintained for 4 days at which time they were fixed and stained with Oil Red O.

Calvarial Osteoblast Culture

Calvarial osteoblasts (COB) were isolated from wildtype and *Misty* neonates (P3) as previously described (34). Briefly, calvariae were digested with collagenase P and trypsin and plated in DMEM supplemented with 10% FBS, and nonessential amino acids. Osteoblastogenesis of primary COB was induced with 8 mM β-glycerophosphate and 50 μg/mL of ascorbic acid in αMEM at confluence (day 7) and maintained until day 21.

Real-time PCR

Total RNA was prepared using an RNeasy Mini Kit (Qiagen, Valencia, CA) for cell culture samples or using standard TRIZOL (Sigma, St. Louis, MO) method for tissues. cDNA was generated using a random hexamer and reverse transcriptase (Superscript III, Invitrogen, Carlsbad, CA) according to the manufacturer's instructions. mRNA expression analysis was carried out using an iQ SYBR Green Supermix with an iQ5 thermal cycler and detection system (Bio-Rad, Hercules, CA). *Hprt* was used as an internal standard control gene for all quantification (35). Primers were designed and tested to be 95–100% efficient by PrimerDesign (Southampton, UK) unless otherwise noted. All primer sequences are listed in Supplementary Table S1.

Propranolol Treatment

Propranolol (Roxane Laboratories, Columbus, OH) was administered at a concentration of 0.5 mg/ml in the drinking water of female *Misty* and control mice for 8 weeks, from 12–20 weeks of age. Propranolol-containing water was replaced three times per week. Untreated *Misty* and control mice had normal drinking water.

Serum Parameters

Serum concentrations of P1NP and CTx were measured with the Rat/Mouse P1NP EIA and the RatLaps EIA, respectively (Immunodiagnostic Systems, Scottsdale, AZ). The assay sensitivities were 0.7 and 2 ng/ml for P1NP and CTx, respectively. The intraassay variations were 6.3% and 6.9% and the interassay variations were 8.5% and 12%, respectively for both assays. All measurements were performed in duplicate.

Indirect Calorimetry

Indirect calorimetry measurements were performed using the Promethion® Metabolic Cage System (Sable Systems, Las Vegas, NV) located in the Physiology Core Department of Maine Medical Research Institute. Mice were subjected to a standard 12 hr light/dark cycle during the study which consisted of a 12 hr acclimation period followed by a 72 hour sampling duration. Data shown are representative of the 24 hr average of this period. Each cage in the 8 cage system consists of a cage with standard bedding, a food hopper, water bottle and "house- like enrichment tube" for body mass measurements connected to load cells for continuous monitoring as well as a 11.5 cm running wheel connected to a magnetic reed switch to record revolutions. Ambulatory activity and position were monitored using the XYZ beam arrays with a beam spacing of 0.25 cm. Respiratory gases were measured using the GA-3 gas analyzer (Sable Systems, Las Vegas, NV) utilizing a pull-mode, negative pressure system. Air flow is measured and controlled by the FR-8 (Sable Systems, Las Vegas, NV), with a set flow rate of 2000 mL/min. Oxygen consumption and carbon dioxide production were reported in mL/min. Water vapor is continuously measured and its dilution effect on O_2 and CO_2 are mathematically compensated for in the analysis stream

(36). Energy expenditure was calculated using the Weir equation: Kcal/hr = $60*(0.003941*VO_2+0.001106*VCO_2)$ and respiratory quotient (RQ) was calculated as the ratio of VCO_2/VO_2. Ambulatory activity and wheel running were determined simultaneously with the collection of the calorimetry data. Data acquisition and instrument control were performed using the MetaScreen software v. 1.7.2.3 and the obtained raw data was processed using ExpeData v. 1.5.4 (Sable Systems, Las Vegas, NV) using an analysis script detailing all aspects of data transformation. Correlations were performed between energy expenditure and lean, fat and total body mass to determine if these variables could explain changes in energy expenditure (37–39).

Western Blot

Tibiae were isolated from female *Misty* and wildtype mice at 8 wks of age, flash frozen, and crushed under liquid nitrogen conditions. Particulates were incubated for 5 minutes at 95°C in Laemmli buffer and protein concentration of the supernatant was determined by BCA assay. Protein (31μg) of wildtype and *Misty* bone lysates was electrophoresed on 4–15% Tris-glycine gel and transferred to an Immun-Blot PVDF membrane for western blot analysis. Blots were probed with antibodies to DOCK7 (1:1000) (22), β-actin (1:10,000), ECL™-peroxidase labeled anti-rabbit HRP (1:2000), and ECL™-peroxidase labeled anti-mouse HRP (1:10,000).

Statistical analysis

All data are expressed as the mean ± standard error of the mean (SEM) unless otherwise noted. Results were analyzed for statistically significant differences using Student's *t*-test or ANOVA followed by Bonferroni's multiple comparison *posthoc* test where appropriate. All statistics, including regression analysis, were performed with Prism 6 statistical software (GraphPad Software, Inc. La Jolla, CA). Statistical significance was set at $p<0.05$.

Results

Misty mice are small with less fat-free mass

To initially examine body composition of *Misty* mice, we performed DEXA measurements for lean, fat and bone mass (Figure 1). Female *Misty* mice had approximately 10% lower body mass than wildtype at 4, 8, 12 and 16 weeks. This difference could be largely accounted for by reduced fat-free mass. Interestingly, fat mass in *Misty* mice varied depending on age, with significantly higher fat mass at 8 weeks and lower fat mass at 16 weeks. Both total and femoral areal bone mineral density (aBMD) and bone mineral content (aBMC) were significantly lower in *Misty* compared to wildtype at all time points examined (femoral aBMD data not shown). Male *Misty* mice had similar defects in body composition as the female mice (not shown).

Trabecular bone loss is accelerated in *Misty* from 8 to 16 weeks of age

Female *Misty* mice have significantly lower distal femur trabecular BV/TV (Tb.BV/TV) compared to wildtype at both 8 and 16 weeks of age (Table I and Figure 2), with lower connectivity density (Conn.D) and trabecular number (Tb.N), as well as increased trabecular separation. Trabecular thickness (Tb.Th) was not different between wildtype and *Misty* at either age. Two-way analysis of variance (ANOVA) demonstrated a significant genotype-age interaction in both the BV/TV and connectivity density parameters. Thus, Tb.BV/TV declined 63% between 8 and 16 weeks of age in *Misty*, whereas it declined only by 49% in wildtype mice over the same period. Similar to females, male *Misty* mice also had low distal femur Tb.BV/TV at 8 and 16 weeks of age (Table S2). However, the acceleration in bone loss with age was not present in male mice.

In female *Misty* L5 vertebrae, Tb.BV/TV was significantly lower than wildtype at both 8 and 16 weeks (Table I). Remarkably, at 20 weeks of age vertebral BV/TV was more than 50% lower than age-matched wildtype controls (Table S4). Similar to the femur, connectivity density and trabecular number were significantly reduced while trabecular spacing was elevated in *Misty* vertebrae. Additionally, trabecular thickness was significantly reduced at the 16-week time point only. Two-way ANOVA did not demonstrate a significant interaction between genotype and age in any of the vertebral parameters.

Cortical thickness was significantly lower in female *Misty* femur midshaft than in wildtype at both ages (Table I). Although mid-femoral cross-sectional area was higher in *Misty* at 8 weeks of age compared to wildtype, mid-femoral cross-sectional area was not different between wildtype and *Misty* at 16 weeks of age, suggesting impaired periosteal expansion. Similar to trabecular bone mass, changes in cortical bone from the *Misty* mutation were not as profound, albeit still significant, in males compared to females (Table S2).

Trabecular bone changes are attributable to both reduced bone formation and increased resorption

To determine which components of the basic multicellular unit were affected by the *Misty* mutation, we performed static and dynamic histomorphometry on the proximal tibia of both female and male mice at 16 weeks of age. Changes in trabecular microarchitecture by histomorphometry (not shown) were consistent with those from μCT (Table I). Percent mineralized surface (MS/BS), bone formation rate (BFR/BS), osteoblast number (N.Ob/B.Pm) and osteoid thickness were markedly reduced in *Misty* compared to wildtype, although the mineral apposition rate did not differ by genotype. Additionally, osteoclast surface (Oc.S), osteoclast number (N.Oc/B.Pm) and percent eroded surface (ES/BS) were all significantly elevated. *Misty* bone marrow also had 63% more adipocytes than wildtype marrow. Thus, a marked reduction in the number of osteoblasts recruited to the bone surface, as well as an increase in osteoclast number and activity accounts for the trabecular bone changes in *Misty* female mice. *Misty* male mice had increased osteoclast surface and osteoclast number, but did not have altered osteoblast parameters compared to wildtype at 16 weeks of age, which could account for the less profound trabecular bone loss phenotype in males (Table S2). To fully understand the mechanism of low bone mass in *Misty,* the remaining studies were performed primarily in female mice.

Interscapular brown adipose tissue is present, but less functional, in *Misty* mice

To examine whether the absence of brown fat previously described in *Misty* could alter bone metabolism, we first set out to confirm the absence of pre-formed brown fat (21). To our surprise, *Misty* mice did indeed have measureable interscapular brown adipose tissue (BAT), which was not different in size, but more variable in *Misty* compared to wildtype (Figure 3A). *Misty* BAT tended to have more lipid droplets and less UCP-1 staining (Figure 3B,C). To determine whether the BAT present in Misty was functional, we used infrared imaging to examine the temperature of the interscapular region. Despite a normal core temperature, the interscapular surface temperature was significantly lower in *Misty* compared to wildtype at 12 weeks of age (Figure 3D,E). Interestingly, stimulation of BAT function with the β3 adrenergic receptor agonist BRL37344 resulted in increased interscapular temperature and increased *Pgc1a* in both genotypes, indicating *Misty* BAT is responsive to direct activation (Figure 3F,G). Although it appears that the BRL37344-induced temperature and *Pgc1a* increases are slightly higher in *Misty* compared to wildtype, there are no significant genotype X treatment interactions by two-way ANOVA (p=0.61 and p=0.35, respectively). We hypothesized that the reduced BAT temperature at baseline could be the result of impaired sympathetic signaling to BAT, so we quantified sympathetic nerve fibers in wildtype and *Misty* BAT. The number of tyrosine hydroxylase (TH) positive fibers

was significantly reduced in *Misty* BAT compared to wild type (Figure 3 H,I). To determine whether DOCK7 could play a cell autonomous role in BAT, we differentiated primary brown adipocytes from the stromal vascular fraction of the interscapular BAT of wildtype and *Misty* mice but found no difference in Oil Red O staining between the two groups (Figure 3J).

Misty white adipose tissue has an elevated response to cold exposure

To determine whether the observed reduction in BAT temperature and sympathetic innervation had physiologic consequences we exposed wildtype and *Misty* mice to cold (4°C) for 6 hours. After an initial drop in core temperature, both genotypes maintained core temperature at approximately 37°C throughout the experiment (Figure 4A). BAT expression of *Pgc1a* was increased in both genotypes compared to ambient temperature controls, however the level of expression in cold-exposed *Misty* mice did not reach that of cold-exposed wild type, likely due to a significant reduction in baseline *Pgc1a* expression (Figure 4B). In order to maintain core temperature in the presence of significantly lower BAT temperature, sympathetic innervation and *Pgc1a* expression, we hypothesized that *Misty* mice must compensate through another mechanism of heat generation. Indeed, inguinal white adipose tissue (WAT) from cold-exposed *Misty* mice had increased expression of genes associated with "browning" of white adipose tissue (*Pdk4, Foxc2, Pgc1a* and *Acadl*) compared to ambient temperature controls (Figure 4C). Inguinal WAT from wildtype mice did not show the same increases noted in Misty. Interestingly, the elevation of *Pgc1a* and *Acadl* in cold-exposed *Misty* occurred despite significantly lower baseline (room temperature) expression of these genes in *Misty* compared to wildtype.

Bone responds to cold temperature

Browning of WAT is under the control of the sympathetic nervous system, therefore, we hypothesized that *Misty* mice have elevated sympathetic tone, which could partially account for their low trabecular bone volume and accelerated trabecular bone loss after 8 weeks of age. We tested this hypothesis with two strategies. First, to examine whether bone metabolism responds to cold, we measured whole tibia gene expression of bone markers after cold exposure. *Runx2* was significantly suppressed by cold in both wildtype and *Misty* mice (Figure 4D). Furthermore, expression of the osteoclast recruitment factor *Rankl* was elevated by cold exposure in *Misty*, but not wildtype tibiae.

Increased sympathetic tone accounts for accelerated trabecular bone loss in *Misty* femur

To test whether elevated sympathetic activity could cause bone loss under ambient conditions as *Misty* mice age, we treated wildtype and Misty mice with the non-selective β2 adrenergic receptor (β2AR) antagonist propranolol, which would block sympathetic signaling at the level of the osteoblast. Although propranolol did not alter bone mass in wildtype mice, it increased total bone mineral content (BMC) accrual and slowed distal femur trabecular bone loss in *Misty* mice from 12 to 20 weeks of age (Figure 5A–C). Increased Tb.Th and Tb.N accompanied the high trabecular BV/TV in *Misty* mice treated with propranolol (Figure 5D,E). Interestingly, trabecular BV/TV was significantly increased in vertebrae from both wildtype and *Misty* mice treated with propranolol (Table S4). Additionally, propranolol suppressed the marker of bone resorption, serum Ctx, in *Misty* mice but not wildtype (Figure 5F). Propranolol did not alter serum P1NP, the marker of bone formation, in either wildtype or *Misty* mice (Figure 5G).

Low energy expenditure in *Misty* mice is due to decreased muscle mass

We hypothesized that high sympathetic tone in *Misty* would be accompanied by increased energy expenditure, so we measured energy expenditure of *Misty* and wildtype female mice

at 8 and 16 weeks of age. Contrary to our initial hypothesis, *Misty* mice had significantly lower energy expenditure (EE) at 8 weeks (Table III) and 16 weeks (data not shown). On the other hand, energy expenditure was significantly and directly related to fat-free mass (r^2=0.971, Table IV and Figure S1). Hence, we suspected that the low EE was related to reduced lean/muscle mass in *Misty* mice. Consistent with this, when EE was divided by fat-free mass, the difference between the two genotypes disappeared (29.3 ± 0.3 kcal/kg*hr in wildtype vs. 28.8 ± 0.2 kcal/kg*hr in *Misty*, p=0.40). To confirm altered muscle mass in *Misty* mice, we weighed soleus, gastrocnemius and thigh muscle in 8-week-old wildtype and *Misty* mice. Gastrocnemius and thigh muscles from *Misty* mice weighed significantly less than wildtype, consistent with the reduced fat-free mass and energy expenditure noted previously (Table III).

DOCK7 has a significant role in osteoblast function

Although sympathetic tone was higher in *Misty* mice and this could be linked to lower bone mass, it appeared unlikely that the increase in sympathetic activity could account for the marked reduction in the recruitment of osteoblasts, nor the fact that bone mass in *Misty* mice was reduced as early as 4 weeks of age (Figure 1). Therefore, we hypothesized that the protein mutated in *Misty* mice, DOCK7, could have a cell autonomous role that had not been previously described in osteoblasts. First we found that the DOCK7 protein is detectable in whole femur lysates and *Dock7* mRNA is detectable in calvarial osteoblasts (Figure 6) as well as in MC3T3-E1 cells at all stages of differentiation (not shown). Second, although mRNA for *Dock7* is detectable in *Misty* mice (Figure 6A), protein expression (using an N-terminal antibody to an epitope of DOCK7 upstream of the truncation) is absent in whole bone lysates from *Misty* mice (Figure 6B). Additionally, we did not detect a protein product at or near the predicted 76 kDa molecular weight that we would expect if indeed a truncated DOCK7 protein was being produced. Consistent with reduced osteoblast number *in vivo* (Table II), bone marrow stromal cell cultures derived from *Misty* mice had significantly lower colony forming units (CFU-F) compared to those derived from wildtype (data not shown). Similarly, primary calvarial osteoblasts from *Misty* neonates had reduced alkaline phosphatase staining at day 7 and 21 and reduced Von Kossa stained mineral at day 21 compared to wildtype (Figure 6C). Although the early osteoblast marker *Runx2* was unchanged, expression levels of alkaline phosphatase and osteocalcin were both reduced at day 21 (Figure 6D). Taken together, these data support the tenet that DOCK7 plays an important role in osteoblast recruitment and differentiation and that in the *Misty* mice there are both cell autonomous and non-cell autonomous effects which contribute to low bone mass.

Discussion

Although accumulating evidence demonstrates that skeletal metabolism is under the control of systemic energy balance and that sympathetic tone plays an integral role in this regulation (1, 40, 41), the role of BAT in bone remodeling is not well understood. *Misty* mice were originally described as having no brown adipose tissue (21); hence our rationale for testing the effect of BAT on bone mass. However, we determined that BAT is indeed present, albeit partially functional (Figure 3). Notwithstanding, we hypothesized that BAT dysfunction could increase sympathetic signaling to bone and cause uncoupled skeletal remodeling. Indeed, *Misty* mice do have low trabecular and cortical bone mass that is likely due to a combination of cell-autonomous and indirect (sympathetically mediated) effects. Additionally, we demonstrate for the first time that bone responds, albeit adversely, to cold temperature, even in wildtype B6 mice.

BAT, which is present in neonates, was thought to become non-functional by adulthood; however, accumulating evidence from PET scanning suggests the existence of functional

BAT in many adults (11–14). Moreover, stimulation of BAT activity has become a potential target for new drugs to combat obesity (42). Nevertheless, it remains to be elucidated whether BAT dysfunction is involved in the pathogenesis of diseases involving altered energy metabolism such as obesity. UCP-1 is critical for brown fat function, serving as the uncoupling protein in mitochondria necessary for proton transfer and heat generation. *Ucp1*$^{-/-}$ mice gained weight and fat mass when placed at thermoneutrality on a high fat diet, but became resistant to diet-induced obesity when the ambient temperature was decreased (43, 44). This is best explained by the activation of an alternative thermogenic program induced to maintain body temperature and through sympathetic stimulation that increases the metabolic rate in non-BAT tissues. However, the thermogenic capacity of non-BAT tissues is not as efficient as BAT, and requires more calories to maintain body temperature, resulting in the increased energy expenditure and decreased adiposity of some animal models. Similar to *Ucp1*$^{-/-}$ mice, *Misty* mice had reduced body temperature and increased markers of thermogenesis in WAT in response to cold (Figure 4), suggesting this alternative thermogenic network is likely activated (45, 46).

It is now well established that skeletal metabolism is under the regulation of the central nervous system, which is mediated through the modulation of sympathetic tone (1). Pharmacological activation of the β2 adrenergic receptor has been shown to result in low bone mass, whereas pharmacological suppression can increase bone mass in certain individuals, suggesting that activation of sympathetic nervous system is a negative regulator for bone mass. In line with this, both global β2-adrenergic receptor (*Adrb2*) knockout mice, and osteoblast conditionally deleted *Adrb2* mice have high bone mineral density (9, 47). Activation of the sympathetic nervous system stimulates bone resorption in part by increasing the expression of *Rankl* in osteoblasts, whereas it suppresses bone formation, thus uncoupling the bone remodeling unit and causing bone loss (9). In our study, the low bone mass phenotype of *Misty* mice was accompanied by uncoupling of bone remodeling; i.e. impaired bone formation and increased bone resorption, which resembles the skeletal characteristics of the mice treated with β-adrenergic agonists. Importantly, blockade of β-adrenergic sympathetic tone slowed, although did not totally reverse trabecular bone loss in *Misty* mice (Figure 5). These lines of evidence demonstrate that elevated sympathetic tone is in part responsible for the reduced bone mass phenotype in *Misty* mice.

Although *Misty* mice showed a remarkable age-dependent bone loss phenotype, areal BMD in *Misty* mice was impaired as early as 4 weeks of age (Figure 1) and trabecular bone mass was not completely rescued by propranolol treatment (Figure 5), suggesting that the *Misty* mutation in DOCK7 contributes to the skeletal phenotype independent of sympathetic tone. Indeed, calvarial osteoblast differentiation was impaired in *Misty* mice compared with controls (Figure 6), which is consistent with reduced osteoblast numbers and percent mineralizing surface *in vivo* (Table II). A function for DOCK7 in osteoblasts has not been previously described. However, others have demonstrated that DOCK7 is important for axon specification and ErbB2-dependent Schwann cell migration (22, 23). DOCK7 knockdown in radial glial progenitor cells suppresses differentiation while overexpression promotes differentiation to neurons (48). We expect that a loss of function of DOCK7 in osteoblasts precursors could affect migration, adhesion and differentiation and a better understanding of these processes could have important physiologic and pathophysiolgic consequences. Thus, a cell-autonomous effect of a presumed loss of function of *Dock7*, together with an increase in sympathetic tone contribute to the remarkable skeletal phenotype in *Misty* mice.

Although activation of thermogenesis in WAT is under the control of the SNS and increases energy expenditure in WAT itself, total body energy expenditure was lower in *Misty* mice compared to wildtype due to a dramatic reduction in fat-free mass, specifically skeletal muscle (Tables III-IV, Figure S1). Whether the *Dock7* mutation in *Misty* mice has a direct

effect on muscle development remains to be clarified, and we therefore cannot exclude that some of the low bone mass in *Misty* could be explained by reduced muscle mass and/or strength.

In sum, we have proposed a novel concept that skeletal metabolism is influenced by BAT function, through modulation of the sympathetic nervous system. Several lines of evidence suggest that sympathetic tone increases with age and in one large cohort study, higher heart rate was a strong and independent predictor of hip fracture risk (49). Moreover, PET imaging suggests that BAT function decreases in older individuals (50). Given the possibility that BAT dysfunction could affect age-related bone loss, beta blockade to enhance bone mass may be a plausible therapeutic target for some individuals with increased SNS tone. Moreover, recent attention has been given to the induction of thermogenesis in WAT to fight obesity. Our findings suggest that targeting thermogenesis may have negative bone consequences, which should be further investigated when developing therapeutics.

Supplementary Material

Refer to Web version on PubMed Central for supplementary material.

Acknowledgments

This work was supported by NIH grants AR061932 to KJM, AG040217 to CJR, AR045433 to CJR, DK084970 to CJR. This work was also supported by NIH grants P20 RR18789 and P20 RR15555 to Don M. Wojchowski and P30 RR030927 to Robert Friesel, and by institutional support from Maine Medical Center. The authors thank Leslie Kozak for experimental input and Linda Van Aelst for the DOCK7 antibody. The authors thank Terry Henderson, David Maridas, Casey Doucette and the Investigative Histopathology Laboratory at Michigan State University for technical assistance and Anyonya Guntur for critical reading of the manuscript.

Funding sources: AR061932 to KJM, AG040217 to CJR, AR045433 to CJR, DK084970 to CJR.

References

1. Takeda S, Elefteriou F, Levasseur R, Liu X, Zhao L, Parker KL, Armstrong D, Ducy P, Karsenty G. Leptin regulates bone formation via the sympathetic nervous system. Cell. 2002 Nov 1; 111(3):305–17. [PubMed: 12419242]
2. Fulzele K, Riddle RC, DiGirolamo DJ, Cao X, Wan C, Chen D, Faugere MC, Aja S, Hussain MA, Bruning JC, Clemens TL. Insulin receptor signaling in osteoblasts regulates postnatal bone acquisition and body composition. Cell. 2010 Jul 23; 142(2):309–19. [PubMed: 20655471]
3. Ferron M, Wei J, Yoshizawa T, Del Fattore A, DePinho RA, Teti A, Ducy P, Karsenty G. Insulin signaling in osteoblasts integrates bone remodeling and energy metabolism. Cell. 2010 Jul 23; 142(2):296–308. [PubMed: 20655470]
4. Friedman JM. Leptin at 14 y of age: an ongoing story. Am J Clin Nutr. 2009 Mar; 89(3):973S–9S. [PubMed: 19190071]
5. Yadav VK, Oury F, Suda N, Liu ZW, Gao XB, Confavreux C, Klemenhagen KC, Tanaka KF, Gingrich JA, Guo XE, Tecott LH, Mann JJ, Hen R, Horvath TL, Karsenty G. A serotonin-dependent mechanism explains the leptin regulation of bone mass, appetite, and energy expenditure. Cell. 2009 Sep 4; 138(5):976–89. [PubMed: 19737523]
6. Yadav VK, Karsenty G. Leptin-dependent co-regulation of bone and energy metabolism. Aging (Albany NY). 2009 Nov; 1(11):954–6. [PubMed: 20157577]
7. Shi Y, Yadav VK, Suda N, Liu XS, Guo XE, Myers MG Jr, Karsenty G. Dissociation of the neuronal regulation of bone mass and energy metabolism by leptin in vivo. Proc Natl Acad Sci U S A. 2008 Dec 23; 105(51):20529–33. [PubMed: 19074282]
8. Ducy P, Amling M, Takeda S, Priemel M, Schilling AF, Beil FT, Shen J, Vinson C, Rueger JM, Karsenty G. Leptin inhibits bone formation through a hypothalamic relay: a central control of bone mass. Cell. 2000 Jan 21; 100(2):197–207. [PubMed: 10660043]

9. Elefteriou F, Ahn JD, Takeda S, Starbuck M, Yang X, Liu X, Kondo H, Richards WG, Bannon TW, Noda M, Clement K, Vaisse C, Karsenty G. Leptin regulation of bone resorption by the sympathetic nervous system and CART. Nature. 2005 Mar 24; 434(7032):514–20. [PubMed: 15724149]
10. Lee NK, Sowa H, Hinoi E, Ferron M, Ahn JD, Confavreux C, Dacquin R, Mee PJ, McKee MD, Jung DY, Zhang Z, Kim JK, Mauvais-Jarvis F, Ducy P, Karsenty G. Endocrine regulation of energy metabolism by the skeleton. Cell. 2007 Aug 10; 130(3):456–69. [PubMed: 17693256]
11. Nedergaard J, Bengtsson T, Cannon B. Unexpected evidence for active brown adipose tissue in adult humans. Am J Physiol Endocrinol Metab. 2007 Aug; 293(2):E444–52. [PubMed: 17473055]
12. van Marken Lichtenbelt WD, Vanhommerig JW, Smulders NM, Drossaerts JM, Kemerink GJ, Bouvy ND, Schrauwen P, Teule GJ. Cold-activated brown adipose tissue in healthy men. N Engl J Med. 2009 Apr 9; 360(15):1500–8. [PubMed: 19357405]
13. Virtanen KA, Lidell ME, Orava J, Heglind M, Westergren R, Niemi T, Taittonen M, Laine J, Savisto NJ, Enerback S, Nuutila P. Functional brown adipose tissue in healthy adults. N Engl J Med. 2009 Apr 9; 360(15):1518–25. [PubMed: 19357407]
14. Cypess AM, Lehman S, Williams G, Tal I, Rodman D, Goldfine AB, Kuo FC, Palmer EL, Tseng YH, Doria A, Kolodny GM, Kahn CR. Identification and importance of brown adipose tissue in adult humans. N Engl J Med. 2009 Apr 9; 360(15):1509–17. [PubMed: 19357406]
15. Ukropec J, Anunciado RP, Ravussin Y, Hulver MW, Kozak LP. UCP1-independent thermogenesis in white adipose tissue of cold-acclimated Ucp1−/− mice. J Biol Chem. 2006 Oct 20; 281(42): 31894–908. [PubMed: 16914547]
16. Granneman JG, Burnazi M, Zhu Z, Schwamb LA. White adipose tissue contributes to UCP1-independent thermogenesis. Am J Physiol Endocrinol Metab. 2003 Dec; 285(6):E1230–6. [PubMed: 12954594]
17. Grujic D, Susulic VS, Harper ME, Himms-Hagen J, Cunningham BA, Corkey BE, Lowell BB. Beta3-adrenergic receptors on white and brown adipocytes mediate beta3-selective agonist-induced effects on energy expenditure, insulin secretion, and food intake. A study using transgenic and gene knockout mice. J Biol Chem. 1997 Jul 11; 272(28):17686–93. [PubMed: 9211919]
18. Bredella MA, Fazeli PK, Freedman LM, Calder G, Lee H, Rosen CJ, Klibanski A. Young women with cold-activated brown adipose tissue have higher bone mineral density and lower Pref-1 than women without brown adipose tissue: a study in women with anorexia nervosa, women recovered from anorexia nervosa, and normal-weight women. J Clin Endocrinol Metab. 2012 Apr; 97(4):E584–90. [PubMed: 22259053]
19. Ponrartana S, Aggabao PC, Hu HH, Aldrovandi GM, Wren TA, Gilsanz V. Brown adipose tissue and its relationship to bone structure in pediatric patients. J Clin Endocrinol Metab. 2012 Aug; 97(8):2693–8. [PubMed: 22593587]
20. Motyl KJ, Rosen CJ. Temperatures rising: brown fat and bone. Discov Med. 2011 Mar; 11(58): 179–85. [PubMed: 21447277]
21. Sviderskaya EV, Novak EK, Swank RT, Bennett DC. The murine misty mutation: phenotypic effects on melanocytes, platelets and brown fat. Genetics. 1998 Jan; 148(1):381–90. [PubMed: 9475748]
22. Watabe-Uchida M, John KA, Janas JA, Newey SE, Van Aelst L. The Rac activator DOCK7 regulates neuronal polarity through local phosphorylation of stathmin/Op18. Neuron. 2006 Sep 21; 51(6):727–39. [PubMed: 16982419]
23. Yamauchi J, Miyamoto Y, Chan JR, Tanoue A. ErbB2 directly activates the exchange factor Dock7 to promote Schwann cell migration. J Cell Biol. 2008 Apr 21; 181(2):351–65. [PubMed: 18426980]
24. Blasius AL, Brandl K, Crozat K, Xia Y, Khovananth K, Krebs P, Smart NG, Zampolli A, Ruggeri ZM, Beutler BA. Mice with mutations of Dock7 have generalized hypopigmentation and white-spotting but show normal neurological function. Proc Natl Acad Sci U S A. 2009 Feb 24; 106(8): 2706–11. [PubMed: 19202056]
25. Rossman KL, Der CJ, Sondek J. GEF means go: turning on RHO GTPases with guanine nucleotide-exchange factors. Nat Rev Mol Cell Biol. 2005 Feb; 6(2):167–80. [PubMed: 15688002]
26. Cote JF, Vuori K. GEF what? Dock180 and related proteins help Rac to polarize cells in new ways. Trends Cell Biol. 2007 Aug; 17(8):383–93. [PubMed: 17765544]

27. Miyamoto Y, Yamauchi J. Cellular signaling of Dock family proteins in neural function. Cell Signal. 2010 Feb; 22(2):175–82. [PubMed: 19796679]
28. DeMambro VE, Clemmons DR, Horton LG, Bouxsein ML, Wood TL, Beamer WG, Canalis E, Rosen CJ. Gender-specific changes in bone turnover and skeletal architecture in igfbp-2-null mice. Endocrinology. 2008 May; 149(5):2051–61. [PubMed: 18276763]
29. Bouxsein ML, Boyd SK, Christiansen BA, Guldberg RE, Jepsen KJ, Muller R. Guidelines for assessment of bone microstructure in rodents using micro-computed tomography. J Bone Miner Res. 2010 Jul; 25(7):1468–86. [PubMed: 20533309]
30. Dempster DW, Compston JE, Drezner MK, Glorieux FH, Kanis JA, Malluche H, Meunier PJ, Ott SM, Recker RR, Parfitt AM. Standardized nomenclature, symbols, and units for bone histomorphometry: a 2012 update of the report of the ASBMR Histomorphometry Nomenclature Committee. J Bone Miner Res. 2013 Jan; 28(1):2–17. [PubMed: 23197339]
31. Kawai M, Green CB, Lecka-Czernik B, Douris N, Gilbert MR, Kojima S, Ackert-Bicknell C, Garg N, Horowitz MC, Adamo ML, Clemmons DR, Rosen CJ. A circadian-regulated gene, Nocturnin, promotes adipogenesis by stimulating PPAR-gamma nuclear translocation. Proc Natl Acad Sci U S A. 2010 Jun 8; 107(23):10508–13. [PubMed: 20498072]
32. Fasshauer M, Klein J, Kriauciunas KM, Ueki K, Benito M, Kahn CR. Essential role of insulin receptor substrate 1 in differentiation of brown adipocytes. Mol Cell Biol. 2001 Jan; 21(1):319–29. [PubMed: 11113206]
33. Fasshauer M, Klein J, Ueki K, Kriauciunas KM, Benito M, White MF, Kahn CR. Essential role of insulin receptor substrate-2 in insulin stimulation of Glut4 translocation and glucose uptake in brown adipocytes. J Biol Chem. 2000 Aug 18; 275(33):25494–501. [PubMed: 10829031]
34. Rosen CJ, Ackert-Bicknell CL, Adamo ML, Shultz KL, Rubin J, Donahue LR, Horton LG, Delahunty KM, Beamer WG, Sipos J, Clemmons D, Nelson T, Bouxsein ML, Horowitz M. Congenic mice with low serum IGF-I have increased body fat, reduced bone mineral density, and an altered osteoblast differentiation program. Bone. 2004 Nov; 35(5):1046–58. [PubMed: 15542029]
35. Vengellur A, LaPres JJ. The role of hypoxia inducible factor 1alpha in cobalt chloride induced cell death in mouse embryonic fibroblasts. Toxicol Sci. 2004 Dec; 82(2):638–46. [PubMed: 15375294]
36. Lighton JR, Turner RJ. The hygric hypothesis does not hold water: abolition of discontinuous gas exchange cycles does not affect water loss in the ant Camponotus vicinus. J Exp Biol. 2008 Feb; 211(Pt 4):563–7. [PubMed: 18245633]
37. Kaiyala KJ, Schwartz MW. Toward a more complete (and less controversial) understanding of energy expenditure and its role in obesity pathogenesis. Diabetes. 2011 Jan; 60(1):17–23. [PubMed: 21193735]
38. Arch JR, Hislop D, Wang SJ, Speakman JR. Some mathematical and technical issues in the measurement and interpretation of open-circuit indirect calorimetry in small animals. Int J Obes (Lond). 2006 Sep; 30(9):1322–31. [PubMed: 16801931]
39. Kaiyala KJ, Morton GJ, Leroux BG, Ogimoto K, Wisse B, Schwartz MW. Identification of body fat mass as a major determinant of metabolic rate in mice. Diabetes. 2010 Jul; 59(7):1657–66. [PubMed: 20413511]
40. Farr JN, Charkoudian N, Barnes JN, Monroe DG, McCready LK, Atkinson EJ, Amin S, Melton LJ 3rd, Joyner MJ, Khosla S. Relationship of sympathetic activity to bone microstructure, turnover, and plasma osteopontin levels in women. J Clin Endocrinol Metab. 2012 Nov; 97(11):4219–27. [PubMed: 22948767]
41. Veldhuis-Vlug AG, El Mahdiui M, Endert E, Heijboer AC, Fliers E, Bisschop PH. Bone resorption is increased in pheochromocytoma patients and normalizes following adrenalectomy. J Clin Endocrinol Metab. 2012 Nov; 97(11):E2093–7. [PubMed: 22990094]
42. Tseng YH, Cypess AM, Kahn CR. Cellular bioenergetics as a target for obesity therapy. Nat Rev Drug Discov. 2010 Jun; 9(6):465–82. [PubMed: 20514071]
43. Liu X, Rossmeisl M, McClaine J, Riachi M, Harper ME, Kozak LP. Paradoxical resistance to diet-induced obesity in UCP1-deficient mice. J Clin Invest. 2003 Feb; 111(3):399–407. [PubMed: 12569166]

44. Feldmann HM, Golozoubova V, Cannon B, Nedergaard J. UCP1 ablation induces obesity and abolishes diet-induced thermogenesis in mice exempt from thermal stress by living at thermoneutrality. Cell Metab. 2009 Feb; 9(2):203–9. [PubMed: 19187776]
45. Seale P, Bjork B, Yang W, Kajimura S, Chin S, Kuang S, Scime A, Devarakonda S, Conroe HM, Erdjument-Bromage H, Tempst P, Rudnicki MA, Beier DR, Spiegelman BM. PRDM16 controls a brown fat/skeletal muscle switch. Nature. 2008 Aug 21; 454(7207):961–7. [PubMed: 18719582]
46. Petrovic N, Walden TB, Shabalina IG, Timmons JA, Cannon B, Nedergaard J. Chronic peroxisome proliferator-activated receptor gamma (PPARgamma) activation of epididymally derived white adipocyte cultures reveals a population of thermogenically competent, UCP1-containing adipocytes molecularly distinct from classic brown adipocytes. J Biol Chem. 2010 Mar 5; 285(10):7153–64. [PubMed: 20028987]
47. Bouxsein ML, Devlin MJ, Glatt V, Dhillon H, Pierroz DD, Ferrari SL. Mice lacking beta-adrenergic receptors have increased bone mass but are not protected from deleterious skeletal effects of ovariectomy. Endocrinology. 2009 Jan; 150(1):144–52. [PubMed: 18801900]
48. Yang YT, Wang CL, Van Aelst L. DOCK7 interacts with TACC3 to regulate interkinetic nuclear migration and cortical neurogenesis. Nat Neurosci. 2012 Sep; 15(9):1201–10. [PubMed: 22842144]
49. Kado DM, Lui LY, Cummings SR. Rapid resting heart rate: a simple and powerful predictor of osteoporotic fractures and mortality in older women. J Am Geriatr Soc. 2002 Mar; 50(3):455–60. [PubMed: 11943040]
50. Nedergaard J, Bengtsson T, Cannon B. Three years with adult human brown adipose tissue. Ann N Y Acad Sci. 2010 Nov.1212:E20–36. [PubMed: 21375707]

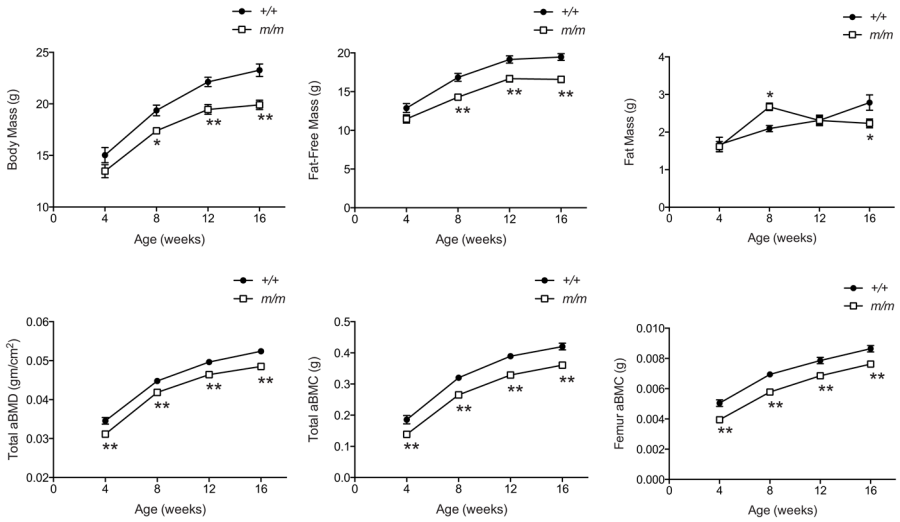

Figure 1. The small size of *Misty* mice can be attributed to reduced fat-free mass and low bone mass

Female *Misty* (open squares) and wildtype (closed circles) littermates were scanned at 4, 8, 12 and 16 weeks of age with a Lunar PIXImus Densitometer for body composition, including total body and femur areal bone mineral density (aBMD) and bone mineral content (aBMC). Points represent mean ± standard error of n=9–15 per group. *p<0.05, **p<0.01 compared to age-matched wildtype.

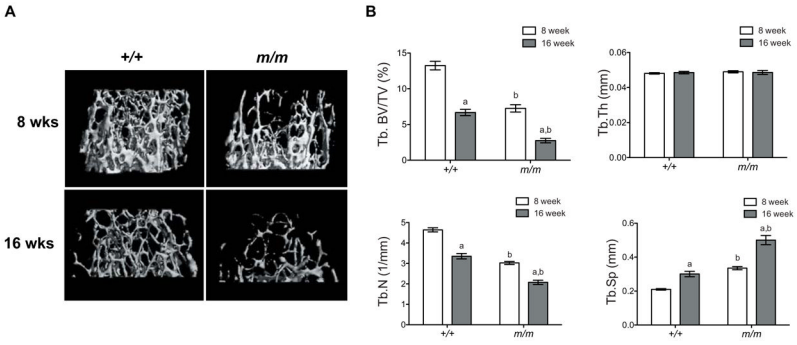

Figure 2. Trabecular bone loss in *Misty* was accelerated with age

(A) Representative images of distal femur microarchitecture, examined in female wildtype (*+/+*) and *Misty* (*m/m*) mice at 8 and 16 weeks of age. (B) Trabecular (Tb.) bone volume fraction (BV/TV), thickness (Th), number (N), separation (Sp) were measured. White (8-week) and gray (16-week) bars represent mean ± standard error. [a]$p<0.05$ compared to genotype-matched 8-week group. [b]$p<0.05$ compared to age matched wildtype group.

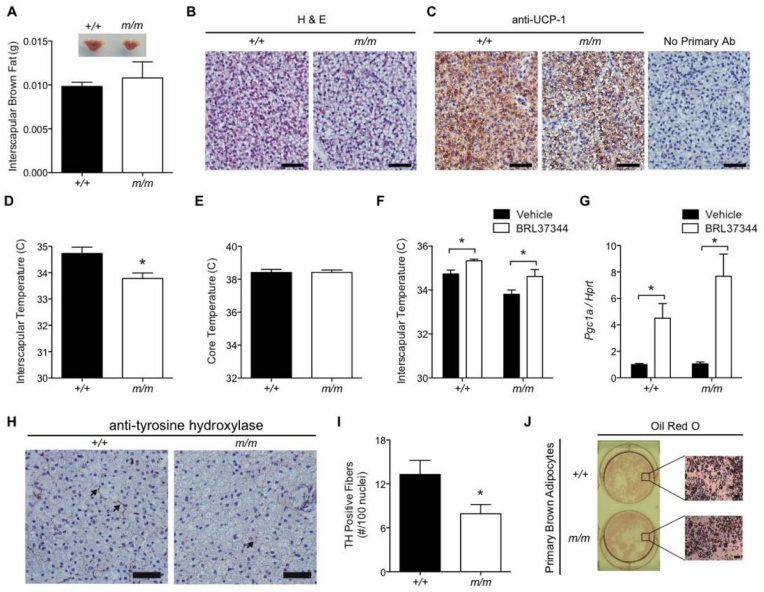

Figure 3. Brown adipose tissue (BAT) is present in *Misty* mice

(A) Interscapular brown adipose tissue was removed from wildtype (*+/+*) and *Misty* (*m/m*) mice at P2 and weighed (n=5–6). (B) Hematoxylin and eosin stain and (C) UCP-1 immunohistochemistry at P2 (n=5–6). Brown stain is positive for UCP-1 and nuclei are blue. (D) Interscapular temperature measured by infrared imaging at 12 weeks of age (n=8) and (E) core temperature measured with a rectal probe at 8 weeks of age (n=10). (F) Interscapular temperature measured by infrared imaging (n=8) and (G) *Pgc1a* expression in interscapular BAT (n= 6–8), 3 hours after injection of vehicle or the β3AR agonist BRL37344. (H) Representative images and (I) quantification of tyrosine hydroxylase (TH) positive sympathetic nerve fibers in BAT from 16 week old *+/+* and *m/m* mice. Brown stain (indicated by black arrows) is positive for tyrosine hydroxylase and nuclei are blue. Three random images from n=5 mice per genotype were quantified. (J) Oil red O stain of primary brown adipocyte culture. Image representative of two experiments performed in triplicate with BAT from 4–6 pups per genotype. Bars represent mean ± standard error. Scale bars = 50 μm.

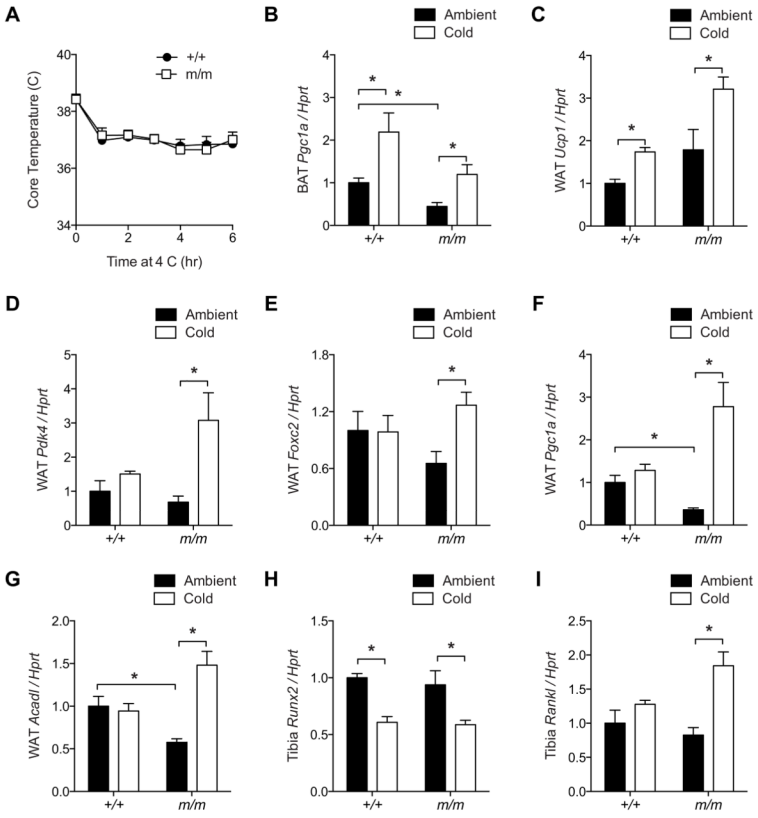

Figure 4. Cold-induced thermogenesis in WAT of *Misty* mice is accompanied by altered gene expression in bone

Eight week old wildtype and *Misty* mice were subjected to 4°C temperature for six hours or maintained at ambient temperature. (A) Rectal temperature of cold-treated mice was measured every hour. (B) *Pgc1a* expression in interscapular BAT. (C–G) *Ucp1*, *Pdk4*, *Foxc2*, *Pgc1a* and *Acadl* expression in inguinal WAT. (H–I) *Runx2* and *Rankl* expression in tibia. N=5–10. *p<0.05.

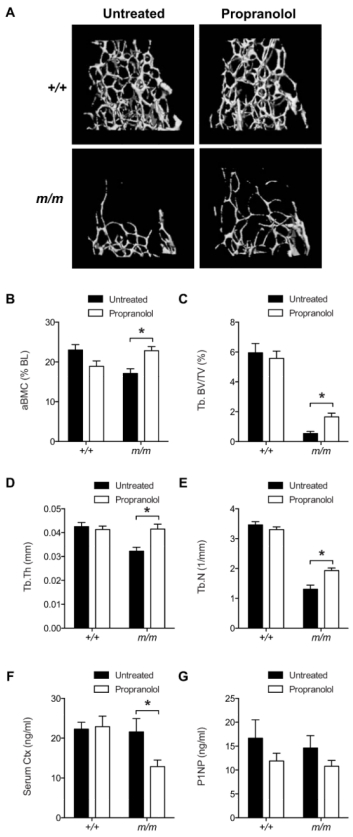

Figure 5. β-adrenergic receptor blockade slows age-related trabecular bone loss in *Misty* mice

Wildtype and *Misty* mice were administered propranolol from 12 to 20 weeks of age. (A) Representative μCT images of the distal femur trabecular bone. (B) aBMC was measured using DEXA. (C–E) Trabecular BV/TV, Tb.Th and Tb.N were measured by μCT. (F–G) Serum Ctx and P1NP were measured by EIA. N=7–9. *p<0.05.

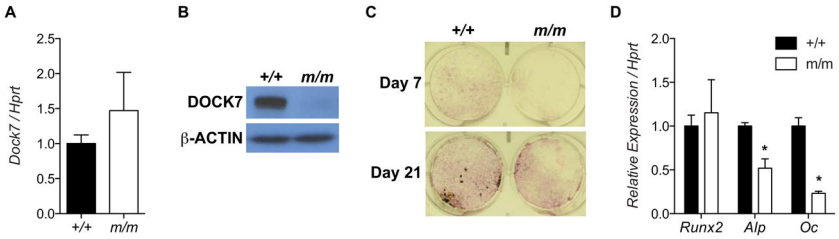

Figure 6. Loss of function of DOCK7 reduces calvarial osteoblastogenesis *in vitro*

Calvarial osteoblasts were isolated from *Misty* and wildtype neonates and differentiated into osteoblasts. (A) *Dock7* expression at day 21. (B) DOCK7 protein expression from whole femur lysates from wildtype and *Misty* mice. (C) Calvarial osteoblast alkaline phosphatase stain at day 7 and alkaline phosphatase and Von Kossa stain at day 21. (D) Expression of osteoblast differentiation markers in calvarial osteoblast cultures at day 21. Gene expression and images representative of two experiments, each performed in triplicate. *p<0.05.

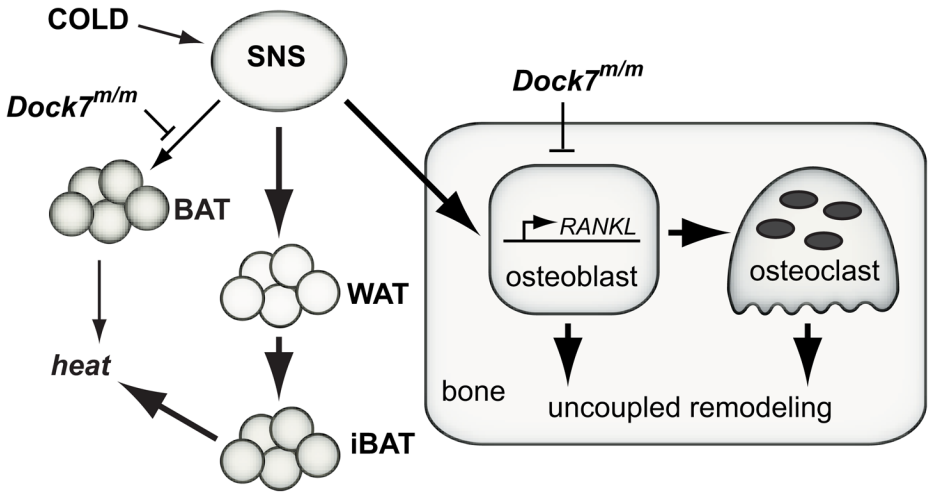

Figure 7. Model of SNS-mediated bone changes in response to cold

Cold temperature induces heat generation in brown adipose tissue (BAT) and inducible BAT (iBAT) if necessary (such as with BAT dysfunction in *Misty* mice). These sympathetically mediated events can also lead to uncoupled skeletal remodeling and accelerated trabecular bone loss with age. Additionally, the *Misty* mutation in *Dock7* has a cell-autonomous role in osteoblasts, through suppression of differentiation.

Table I

μCT of female wildtype and *Misty* femur and vertebrae at 8 and 16 weeks of age.

	8 weeks		16 weeks		2-way ANOVA *p*-value		
	+/+ (n=10)	***m/m* (n=10)**	**+/+ (n=10)**	***m/m* (n=15)**	**Interaction**	**Age**	**Genotype**
Femur Midshaft							
Ct.Th (mm)	0.149 ± 0.003	0.126 ± 0.003 **	0.181 ± 0.004	0.165 ± 0.003 **	0.390	< 0.001	< 0.001
Tt.Ar (mm^2)	1.10 ± 0.02	1.24 ± 0.02 **	1.78 ± 0.03	1.78 ± 0.03	0.011	< 0.001	0.008
Ct.Ar (mm^2)	0.65± 0.02	0.56 ± 0.01 **	0.77 ± 0.02	0.70 ± 0.02 *	0.555	< 0.001	< 0.001
Ct.Ar/Tt.Ar (%)	37.3 ± 0.5	31.2 ± 0.6 **	43.5 ± 0.7	39.7 ± 0.6 **	0.122	< 0.001	< 0.001
Distal Femur							
BV/TV (%)	13.2 ± 0.6	7.3 ± 0.5 **	6.7 ± 0.4	2.7 ± 0.3 **	0.031	< 0.001	< 0.001
Conn.D ($1/mm^3$)	132 ± 9	54 ± 7 **	52 ± 6	9 ± 2 **	0.006	< 0.001	< 0.001
Tb.N (1/mm)	4.64 ± 0.10	3.03 ± 0.07 **	3.35 ± 0.13	2.08 ± 0.13 **	0.123	< 0.001	< 0.001
Tb.Th (mm)	0.048 ± 0.000	0.049 ± 0.001	0.049 ± 0.001	0.049 ± 0.001	0.636	0.965	0.559
Tb.Sp (mm)	0.210 ± 0.005	0.335 ± 0.009 **	0.301 ± 0.016	0.500 ± 0.032 **	0.066	< 0.001	< 0.001
Vertebrae (L5)							
BV/TV (%)	26.2 ± 0.6	21.9 ± 0.5 **	24.4 ± 0.6	18.2 ± 1.2 **	0.230	0.001	< 0.001
Conn.D ($1/mm^3$)	199 ± 8	157 ± 7 **	127 ± 7	87 ± 9 **	0.871	< 0.001	< 0.001
Tb.N (1/mm)	5.22 ± 0.09	4.60 ± 0.10 **	4.23 ± 0.10	3.72 ± 0.17 *	0.646	< 0.001	< 0.001
Tb.Th (mm)	0.0503 ± 0.0004	0.0505 ± 0.0003	0.0573 ± 0.0015	0.0557 ± 0.0021 *	0.068	< 0.001	0.148
Tb.Sp (mm)	0.185 ± 0.004	0.209 ± 0.004 **	0.230 ± 0.007	0.264 ± 0.012 *	0.541	< 0.001	0.001

Values are expressed as the mean ± SEM. *Abbreviations:* Ct, cortical; Th, thickness; Tt, total; Ar, area; BV, bone volume; TV, total volume; Conn.D, connectivity density; Tb, trabecular; N, number; Sp, separation.

** p<0.01 *vs* age matched wildtype.

* p<0.05 *vs* age matched wildtype.

Table II

Proximal tibia histomorphometry of female wildtype and *Misty* mice at 16 weeks of age.

	+/+ (n=4–7)	***m/m* (n=7)**
MS/BS (%)	39.3 ± 1.9	24.8 ± 3.5 *
MAR (μm/day)	1.99 ± 0.21	1.34 ± 0.35
BFR/BS($\mu m^3/\mu m^2$/year)	286 ± 38	138 ± 43 *
Ob.S/BS (%)	9.92 ± 3.27	3.08 ± 1.86
N.Ob/B.Pm (/mm)	8.43 ± 2.67	2.03 ± 1.13 *
OS/BS (%)	5.65 ± 2.27	1.32 ± 1.32
O.Th (μm)	2.34 ± 0.75	0.33 ± 0.33 *
Oc.S/BS (%)	1.43 ± 0.26	3.32 ± 0.73 *
N.Oc/B.Pm (/mm)	0.56 ± 0.11	1.50 ± 0.33 *
ES/BS (%)	0.48 ± 0.20	1.87 ± 0.52 *
N.Ad/T.Ar ($/mm^2$)	32.0 ± 4.5	52.3 ± 6.2 *

Abbreviations: MS/BS: mineralized surface/bone surface, MAR: mineral apposition rate, BFR/BS: bone formation rate/bone surface, ObS/BS: osteoblast surface/bone surface, N.Ob/B.Pm: number of osteoblast/bone perimeter, OS/BS: osteoid surface/bone surface, O.Th: osteoid thickness, Oc.S/BS: osteoclast surface/bone surface, N.Oc/B.Pm: number of osteoclasts/bone perimeter, ES/BS: erosion surface/bone surface, N.Ad/T.Ar: number of adipocyte/total area.

N/A: not available

* $p<0.05$ compared to control

** $p<0.01$ compared to control

Table III

Body composition and metabolic variables in 8-week female *Misty* and wildtype mice.

	+/+ (n=4–8)	***m/m* (n=4–8)**	***p*-value**
Body Mass (g)	21.1 ± 0.8	18.3 ± 0.4	0.042
FFM (g)	17.7 ± 0.5	15.2 ± 0.5	0.025
Fat (g)	2.9 ± 0.3	3.1 ± 0.2	0.696
Activity (meters/day)	7241 ± 922	4795 ± 476	0.057
RER	0.847 ± 0.009	0.782 ± 0.039	0.155
EE (Kcal/hr)	0.516 ± 0.02	0.411 ± 0.03	0.020
Thigh (mg)	225 ± 7	201 ± 6	0.017
Gastrocnemius (mg)	91 ± 2	74 ± 2	<0.001
Soleus (mg)	6.2 ± 0.3	6.0 ± 0.9	0.843

Abbreviations: FFM, fat-free mass; RER, respiratory exchange ratio; EE, energy expenditure.

Table IV

Linear regression analysis of total EE vs. body composition in the *Misty* mouse model.

	r^2	*p*-value
Total Body Mass	0.87	0.0023
Fat-Free Mass	0.97	<.0001
Fat Mass	0.04	0.68